Impact of ICRF Fast-Ions on Core Turbulence and MHD Activity in ASDEX Upgrade

R. Bilato,[1, a)] C. Angioni,[1] A. Bañón Navarro,[1] V. Bobkov,[1] T. Bosman,[1] A. Di Siena,[1] E. Fable,[1] R. Fischer,[1] J. Galdon-Quiroga,[2] T. Görler,[1] J. Hidalgo-Salaverri,[3] F. Jenko,[1] T. Johnson,[4] Ye. O. Kazakov,[5] O. Kudlacek,[1] J. Manyer,[6] M. Mantsinen,[6] R. Ochoukov,[1] E. Poli,[1] J.Rueda-Rueda,[7] P.A. Schneider,[1] S. Sipilä,[8] W. Tierens,[1] M. Usoltseva,[1] M. Weiland,[1] ASDEX Upgrade team, and EUROfusion MST1 team

[1)]*Max-Planck-Institut für Plasmaphysik, Boltzmannstr. 2, 85748 Garching, Germany*
[2)]*University of Seville. Avda. Reina Mercedes s/n 41012 Seville, Spain*
[3)]*Dpt. of Energy Engineering, University of Seville, Camino de los Descubrimientos s/n, 41092 Seville, Spain*
[4)]*School of Electrical Engineering, KTH, Stockholm, Sweden*
[5)]*LPP-ERM/KMS, TEC Partner, Brussels, Belgium*
[6)]*ICREA, 0810 Barcelona, Spain*
[7)]*Dept. of Atomic, Molecular and Nuclear Physics, University of Seville, Avda. Reina Mercedes, 41012 Seville, Spain*
[8)]*Department of Applied Physics, Aalto University, PO Box 14100, 00076 AALTO, Finland*

[a)]*Corresponding author: roberto.bilato@ipp.mpg.de*

Abstract. Experiments in various tokamaks and their analysis identify the fast ions (FI) generated by NBI and/or ICRF heating as one of the main causes of the observed improvement in core confinement: fast ions can reduce core microturbulence (mainly Ion-Temperature-Gradient (ITG) driven modes) either electrostatically or electromagnetically, or they can resonate with fishbones and high-frequency Alfvén modes, which in turn contribute in stabilizing ITG. In this perspective, we discuss recent experiments done on ASDEX Upgrade (AUG) where ICRF is the main actuator for FI generation for energies above 100 keV. Additionally, ICRF-FIs can substantially impact the MHD activity and its consequent effects on fast ion losses (FILs) and ion-cyclotron emission (ICE). We present dedicated AUG experiments with NBI-D further accelerated by ICRF.

1. INTRODUCTION

Crucial to reach burning-plasma conditions in a fusion reactor is to achieve reasonable fusion yields in the early phase of the discharge. This implies to reach relatively high ion temperature, T_i, before the discharge flattop, since fusion-cross sections depend strongly on T_i. This should be accomplished mostly with the pedestal in the plasma profiles due to the edge-transport barrier created at the L-H transition triggered by auxiliary heating. However, the performances can improve further if the auxiliary heating is able to increase T_i also directly in the plasma core, the ultimate kern of fusion reactions. The temporal evolution of T_i depends not only on the auxiliary heating entering the ion transport equation as power and particle sources, but also on the heat and particle transport, which in the plasma core are mainly determined by microturbulence (e.g. ITG modes) and by MHD activity (e.g. sawtooth/fishbone, Alfvénic modes), with the latter influencing the former in various subtle ways. Eventually, T_i strongly depends on the sensitivity of the ion heat flux, Q_i, on the logarithm derivative of T_i, $L_{T_i}^{-1} = -\mathrm{d}\ln T_i/\mathrm{d}r$. This sensitivity can be identified with the slope of Q_i as function of R/L_{T_i}, with R the major radius. This slope has a sharp increase at the threshold value $R/L_{T_i}|_c$ corresponding to the onset of microturbulence. Above $R/L_{T_i}|_c$, R/L_{T_i} tends to stay close to $R/L_{T_i}|_c$ limiting further increases of T_i with auxiliary or fusion heating. When turbulent transport is dominant, the ion-heat diffusivity, $\chi_i = Q_i L_{T_i}/(n_i T_i)$, in the ion transport equation can be roughly approximated with the slope χ_i^{stiff} of $Q_i(R/L_{T_i})$ above $R/L_{T_i}|_c$ by writing $\chi_i \approx \chi_i^{\mathrm{stiff}}(1 - L_{T_i}/L_{T_i}|_c)$ for $R/L_{T_i} > R/L_{T_i}|_c$. Therefore, χ_i can be beneficially decreased by either increasing the threshold $R/L_{T_i}|_c$ (upshift) or reducing χ_i^{stiff} (T_i de-stiffening). Gyrokinetic simulations of plasma discharges performed in various fusion devices have shed light on the possible role that fast ions, produced by neutral-beam-injection (NBI) heating and by ion cyclotron radio-frequency (ICRF) heating, might play in up-shifting the threshold $R/L_{T_i}|_c$ and/or (or both) in T_i de-stiffening. Therefore, getting close to the optimal T_i for fusion yield might require an optimized use of the available auxiliary heating and current drive (CD) systems in ITER (NBI, ECRF, ICRF) [1], and in future fusion reactors. This has motivated in the last years a worldwide effort

24th Topical Conference on Radio-frequency Power in Plasmas
AIP Conf. Proc. 2984, 030010-1–030010-10; https://doi.org/10.1063/5.0163029
Published by AIP Publishing. 978-0-7354-4604-5/$30.00

in understanding with both experiments and theory/simulations the impact of auxiliary heating and CD on plasma confinement, with special attention to the role of the fast ions intrinsic to NBI and ICRF heating [2, 3]. Specifically to this topic, in the next section we present ASDEX Upgrade (AUG) experiments performed to address the stabilization of ITG-driven turbulence by resonant ICRF-FIs [4].
In section 3, we briefly report recent measurements on AUG done with fast-ion loss detector (FILD) which show a NBI-induced reduction of the detected fast-ion losses in correspondence of TAEs during ECRF and ICRF heating. Studying fast-ion losses in various mixtures of auxiliary heating is important for ITER and fusion reactors since losses of energetic ions before being thermalized are not only a heating loss but can also locally overheat the plasma facing components (PFC).
Another topic likely relevant for ITER and future fusion reactors is the flattening of core electron temperature, T_e, at increasing NBI power observed in NSTX and explained as electronic transport deterioration caused by global Alfvén eigenmodes (GAE) driven by the same NBI ions when superalfvénic [5]. Since in burning plasmas ion heating by fusion alphas is done indirectly via collisions with electrons on which fusion alphas preferentially slow-down, the impact of GAEs on T_e, and consequently on T_i, might be relevant in the periphery of ITER plasmas where the fusion alphas from the core are superalfvénic and might have the necessary anisotropy in velocity space to excite GAEs. In section 4, we discuss measurements of these modes done with the B-dot probes installed on AUG, and in particular the impact of NBI-FIs further ICRF accelerated on GAEs.

Before proceeding, we recall that AUG is equipped with two pairs of 2-strap (with B-coated limiters) and of 3-strap (with W-coated limiters) antennas which can deliver up to 5 MW. The possible frequencies are 30, 36.5, 41.8 and 55.1 MHz, which allow the D (He^4), H and He^3 fundamental cyclotron resonance for minority and 3-ion heating schemes at typical AUG magnetic field ranging from 1.6 to 3 T. Additionally, high harmonics heating/acceleration of D (2^{nd}, 3^{rd}, and 4^{th}) and H (2^{nd}) is accessible. The pairs of antennas can operate at different frequencies, and this has been used to study the two-step ICRF acceleration of fast ions. Finally, the system offers high flexibility in controlling the phasing between the straps of each antenna and between antennas, and this is an additional degree of freedom in ICRF heating and fast-ion generation [6]. In sections 2 and 3 the ICRF scenario is H-minority heating in D plasmas with NBI-D, whereas in section 4 the scenario is 3^{rd} harmonic of NBI-D.

2. STABILIZATION OF ITG-DRIVEN TURBULENCE BY RESONANT ICRF FAST-IONS

To put into context what is discussed in this section, we briefly summarize a few FI effects on turbulence, and we refer to the recent review [3] for an exhaustive overview and bibliography of the impact of fast ions on turbulence stabilization in tokamaks. Considered as a separate species, FIs dilute the background ion species with the consequence of reducing the main driver of microturbulence due to the background. A second linear electrostatic effect of FIs follows from the FI impact on the geometry of the flux surfaces (Shafranov-shift effect). Because of their large pressure and radial gradients of density, $n_{\rm fi}$, and of equivalent temperature, $T_{\rm fi}$, especially in the case of ICRF-FI, FIs can contribute substantially to increase the MHD parameter $\alpha = -q^2 R(8\pi/B^2)\mathrm{d}p/\mathrm{d}r$ with R the major radius, q the safety factor and B the effective magnetic field strength. This can modify the pressure-gradient driven contribution, $v_{\mathrm{d},\nabla \mathrm{p}}$, to the perpendicular drift velocity (in particular of the background ions, considered here the main ITG driver) at the point to stabilize "bad-curvature" instabilities such as ITG. Moving to non-linear gyrokinetic simulations, saturation of drift-like turbulence generally develops when zonal structures (ZS) - here for both zonal flows (ZF) and zonal currents (ZC) [7] - are excited also by the turbulence itself [8]. These structures work both as siphon of turbulence energy and as tearing mechanism of turbulence eddies, facilitating the cascade of turbulence energy from long to short scale lengths, where it is eventually dissipated. Although this self-regulation mechanism is at play also in the case of nonlinear electrostatic simulations, it is particularly enhanced when electromagnetic effects are turned on in the simulations. This has been recently explained with a three-wave coupling mechanism which increases the energy transfer efficiency from the unstable modes to ZSs via intermediate coupling with stable or marginally stable modes [9]. FIs can contribute to this virtuous circle by increasing the amplitude of the ZSs, and this can happen at least in two ways. First they can excite modes that increase the zonal structure amplitude either directly by exciting ZF through their drift branches or indirectly with their marginal stable modes that increase the triplet correlation time of the EM enhancement discussed previously. A second possibility recognized in [10] appears when the electronic β_e is such to make α close to linear threshold, α_c, for TAE existence [11]. In this case, FIs work as vector for energy transfer from turbulence to marginally stable TAE modes when $\alpha \lesssim \alpha_c$. If the amplitude of TAE modes is large enough, zonal

currents are excited [7] and they add strength to the self-regulation of turbulence, mentioned before. This particular mechanism has been recently found to take place also for linearly unstable TAE modes at JET, if they are kept close to the marginal stability threshold [12]. The story is made much more complicated by other different ways FIs can influence turbulence. For instance, FIs resonant with fishbones (FB) are expelled from inside $q = 1$ during the FB bursts, with a consequent generation of a radial current, which is counterbalanced by an opposite radial current in the bulk plasma necessary to guarantee the divergence-free nature of the total current: This bulk-plasma current sustains a sheared poloidal rotation which contributes to stabilize turbulence when the FB repetition frequency is comparable to the growth rate of ITG modes [13, 14]. In experiments, all these phenomena, and other not mentioned here, are present in different degree of intensity, and it is almost impossible to single them out, even with target experiments. On the other hand, it is feasible to design gyrokinetic simulations to investigate the parameter-dependence of a specific set of mechanisms. However, comprehensive global gyrokinetic simulations that account for all possible mechanisms at the same time are not yet feasible.

Of all the known mechanisms regulating core turbulence due to fast ions [3] (and therein references), here we briefly describe only a wave-particle-resonance type mechanism, which can be particularly effective in the case of ICRF-FIs [4]. A simplified and instructive physical picture of this resonant mechanism can be derived if fast ions are described with an equivalent Maxwellian, $F_{M,\mathrm{fi}}$, characterized by the FI density n_{fi} and the equivalent FI temperature T_{fi}, respictively derived from the zeroth and second order moments of the FI distribution function. The FI contribution is considered perturbatively in the linear electrostatic gyrokinetic equation for the non-adiabatic contribution to the perturbed part of the background ion distribution function. Referring to [15] for the derivation, the contribution of fast ion to the growth rate of the mode $(\omega, \gamma_{\mathbf{k},\omega})$ can be roughly represented as an integral over energy,

$$\frac{\gamma_{\mathrm{fi},\{\mathbf{k},\omega\}}}{\omega} \propto \frac{n_{\mathrm{fi}}}{\varepsilon_{T\mathrm{fi}}} \int \frac{\gamma_{\{\mathbf{k},\omega\}} + \nu}{\left(\omega - \omega_{d,\mathrm{fi}\{\mathbf{k}\}}\right)^2 + \left(\gamma_{\{\mathbf{k},\omega\}} + \nu\right)^2} \left\{ \left[\frac{1}{\eta_{\mathrm{fi}}} + \left(\mathscr{E} - \frac{3}{2} \right) \right] F_{M,\mathrm{fi}}(\mathscr{E}) J_0^2(k_\perp \rho_{\mathrm{fi}} \sqrt{\mathscr{E}}) \mathscr{E}^{3/2} \right\} \mathrm{d}\mathscr{E} \qquad (1)$$

with energy $\mathscr{E}$ normalized to T_{fi}, n_{fi} to the electron density, frequencies to $\omega_{\mathrm{De}} = -ck_y T_e/(eRB)$; ν is an effective

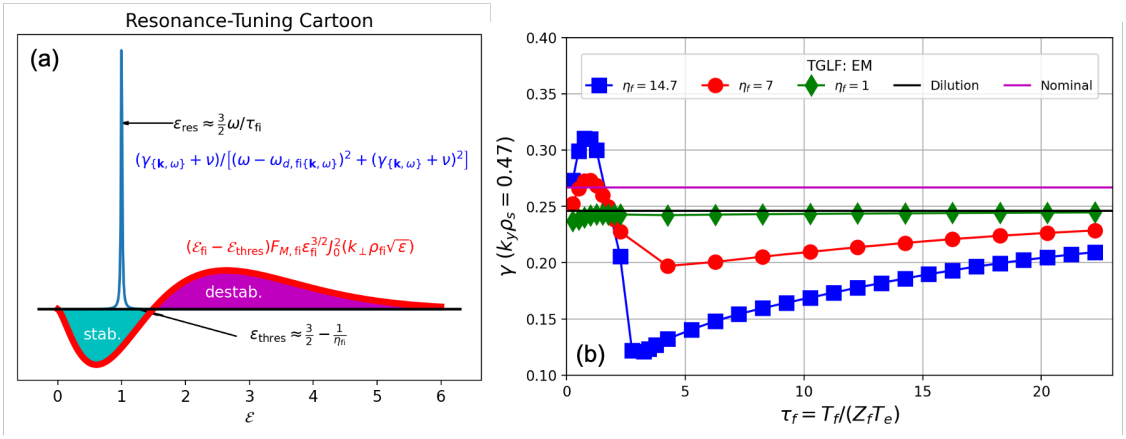

FIGURE 1. (a) Cartoon of the terms in the argument of the integral (1): the first (blue) is a Lorentzian which defines the energy of the fast-ions resonant with the drift mode; the other terms together (red) determine the sign and amplitude of the contribution of fast ions to the growth rate of the mode. (b) The integrals (1) as function of τ_{fi} for a few values of η_{fi}, calculated with TGLF set to high resolution (i.e. with 16 (`nbasis`) Hermite polynomials for the parallel expansion and with 1.85 (`width=width_min`) for the width of the Gaussian measure). The back horizontal line shows the stabilizing effect of dilution.

collisional frequency, $\varepsilon_{n,T} = L_{n,T}/R$, $\eta = L_n/L_T$, $\omega_{d,\mathrm{fi}\{\mathbf{k}\}} \propto (2/3)\tau_{\mathrm{fi}}\mathscr{E}$ the perpendicular ion drift frequency and $\tau = T_i/(Z_i T_e)$ with Z_{i} the ion charge state. Figure 1.a shows the two factors appearing inside the integral of (1). The first factor (blue curve) is a Lorentzian which selects fast ions with $\omega_{d,\mathrm{fi}}$ close to the mode frequency ω (i.e. $\mathscr{E} \approx \omega/\tau_{\mathrm{fi}}$). The second term (red curve) determines the sign (first factor in the brackets of (1)) and amplitude of the fast-ion contribution to the mode growth rate. The width of stabilizing region (negative), $0 \le \mathscr{E} \le 3/2 - \eta_{\mathrm{fi}}^{-1}$, depends on η_{fi}. The control parameter of the Lorentzian (resonance) is τ_{fi} which can make the contribution stabilizing (negative) or destabilizing (positive). Figure 1.b shows an example of how the growth rate of the most unstable mode calculated with the linear solver of TGLF [16] varies with τ_{fi} and η_{fi}. On passing, it is worthwhile to notice that not only TGLF captures this resonant effect but also the TGLF quasilinear model gives trends close to those obtained with fluxtube

GENE simulations [4]. The horizontal magenta line is the growth rate in the absence of fast ions; the black horizontal line shows the growth rate when the dilution effect is included; finally, the symbols are obtained by considering fast-ions as an additional Maxwellian species at different $\eta_{\rm fi}$ values. By increasing $\eta_{\rm fi}$ the effects of fast ions increases and the $\tau_{\rm fi}$ value of optimal stabilization decreases. This dependence on $\eta_{\rm fi}$ makes this mechanism particularly strong in ICRF heating with respect to NBI heating. In fact, the rather localized heating in ICRF makes $L_{T_{\rm fi}}$ smaller than what expected for NBI, and at the same time NBI makes smaller $L_{n_{\rm fi}}$ since it is a source of particles as well. By following Stix's derivation of the equivalent temperature of the ICRF heated species [17], just to grasp the main dependencies of $\tau_{\rm fi}$ we approximately have $\tau_{\rm fi} \propto A_{\rm fi}\,\langle P_{\rm ic}\rangle/(Z_{\rm fi}^3 X_{\rm fi})$, with $X_{\rm fi} = n_{\rm fi}/n_e$ the concentration, $A_{\rm fi}$ and $Z_{\rm fi}$ the atomic mass number and charge, and $\langle P_{\rm ic}\rangle$ the surface-averaged RF power density absorbed by the minority. This stabilization mechanism was likely active in He^3 minority ICRF heating in deuterium plasmas on JET [18] and AUG [19]. To have the same effects with H-minority heating, the H concentration must be higher, about twice the He^3 concentration of the discharges in [19]. For this reason, in the following AUG discharges there was H puffing from the midplane

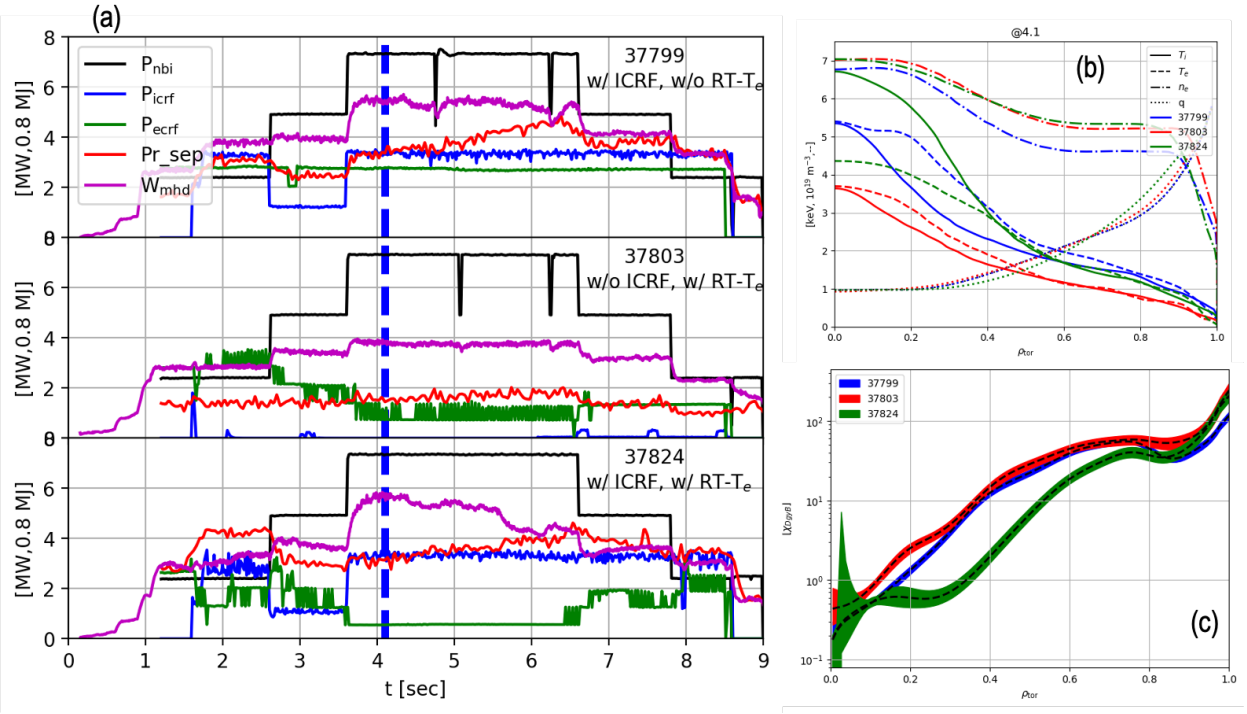

FIGURE 2. (a) Time traces of the auxiliary heating, $W_{\rm mhd}$ and radiated power, $P_{\rm r,sep}$, inside the separatrix [20]. (b) n_e, T_e, T_i and q profiles at 4.1 s, corresponding to the dashed blue vertical line in (a). (c) χ_i profiles normalized to $\chi_{\rm gyB,D}$.

valves to achieve $X_H \approx 8-11\%$ [21]. Here, we discuss a set of three selected discharges which differ either for the ECRF power, $P_{\rm ecrf}$, (37799 vs 37824) or for the presence of ICRF heating, $P_{\rm icrf}$, (37803 vs 37824). Some of the main time traces of these discharges are shown in figure 2.a. The magnetic field B_t is reduced from ≈2.5 T to ≈ 2.4 T between 4.2 s and 5.5 s, and the heating waveforms are symmetric around 5.5 s. In 37803 and 37824, there is a real-time control of T_e (RT-T_e) aiming to keep fix the core T_e at its value determined at about 1.5 s by varying $P_{\rm ecrf}$ [22]. To avoid W accumulation the minimum $P_{\rm ecrf}$ is set to ≈0.5 MW, which is reached immediately in the central part of 37824 at full power, and thus T_e in 37824 is lower than in 37799 but not at level of 37803 (dashed lines in figure 2.b). There are three phases of the auxiliary heating for each value of B_t, and here we are interested at time 4.1 s of maximum auxiliary heating. Despite the lower $P_{\rm ecrf}$ because of the RT-T_e, in 37824 $W_{\rm mhd}$ per MW of input power is larger and T_i definitively higher than in 37799, as shown by the solid lines in figure 2.b. In particular, 37824 has T_e/T_i substantially smaller than one, and the T_i steepening extends from the axis up to $\rho_{\rm tor} \approx 0.5$, around where the q profiles (dotted lines) crosses q=2. The importance of rational-q surfaces on confinement has been observed on JET [23] and AUG [13] in the past. However, the q profile cannot alone explain the differences between 37799 and 37824. Moreover, in all these three discharges there is strong fish-bone activity, and again the MHD activity alone might not be enough here to explain the difference in T_i profiles in figure 2.b. Figure 2.c shows the ion diffusivity

χ_i estimated from the power balance, with the profiles of $P_{\rm ecrf}$ and $P_{\rm icrf+nbi}$ calculated with TORBEAM [24] and TORIC-SSFPQL [25] codes, respectively. In figure 2.c χ_i is normalized to gyro-Bohm diffusivity of deuterium, $\chi_{\rm gyB,D} = (\rho_D/a)(\rho_D^2\Omega_{cD}) = 0.28\,T_i^{3/2}/(aB_t^2)$, with T_i in keV, B_t in Tesla and the minor radius a in meter. The discharges 37799 and 37803 have comparable normalized χ_i up to $\rho_{\rm tor} \approx 0.3$, whereas χ_i of 37799 is lower and it is also where T_i shows a steepening in 37799. On the other hand, the χ_i profile of 37824 is substantially lower than those of 37799 and 37803, from the axis up to $\rho_{\rm tor} \approx 0.8$. With the reduced gyrofluid TGLF [16] model (with SAT2 saturation model) in the transport ASTRA system [26], we froze the auxiliary heating profiles to those calculated with the experimental plasma kinetic profiles, and look for n_e, T_e and T_i that make the fluxes calculated by TGLF match the volume integral of the sources augumented by the energy-equipartition term and radiated power. Figure 3 collects the predicted T_e and T_i profiles for these discharges together with the experimental profiles, the latter in black solid lines. The boundary conditions are imposed at $\rho_{\rm tor} = 0.75$. In 37803 ASTRA/TGLF predictions are close to experimental profiles for T_e and T_i is about 20% larger in the core (blue lines). H concentration estimated by the neutral particle analyzer is about 8%. If the background deuterium is reduced of 8% in TGLF, but not the total ion density in ASTRA, T_e profiles are almost unchanged and T_i ones are slightly larger (magenta lines) than the ones without dilution (blue). This is consistent with the expectation that dilution reduces the driver of the instability. The green and red line in 37799 and 37824 are calculated by considering the H-minority ICRF species as an additional species in TGLF prescribed with a Maxwellian having the temperature shown in dotted red lines and a concentration of 8% with respect to the electron density. The green and red lines are obtained with and without H dilution of the background D in TGLF, respectively. In 37799 T_i calculated w/o FI and dilution (blue) is close to the experimental profile, whereas in 37824 all the estimated T_i profiles are definitively lower in the core than the experimental ones. A common feature in 37799 and 37824 is that the profiles with FI in TGLF (red and green) flattens in the core starting from the point where the derivative of $T_{\rm fi}$ decreases substantially. Here, TGLF called by ASTRA is executed with the usual low resolution, nbasis=6, because of the otherwise prohibitive computational time. This implies that resonant fast-ion effects described in figure 1 are not yet captured in these simulations. In addition to the number of Hermite functions (nbasis), the width and the k_y grid, and the saturation model might need to be tuned to account for the fast-ion effects likely present in these discharges: this might improve ASTRA/TGLF prediction for 37824. In achieving this, a thoroughly analysis with girokinetic codes, such as GENE, in fluxtube (local) mode will be necessary. However, as shown in [21], to properly capture some of the essential effects of unstable FI modes on turbulence, global simulations might be still necessary. These discharges but also other discharges highlight a common feature of the impact of ECRF heating on T_i in the core: in 37799 the higher ECRF power contributes to have $T_e/T_i > 1$ which typically increases turbulent core transport, especially in the ion channel, by increasing the destabilization of ITG modes - this feedback loop helps to sustain $T_e/T_i > 1$. On the other hand, the reduced ECRF power in 37824 might contribute to have $T_e/T_i < 1$ and thus to stabilize ITG with a consequent reduction of ion turbulent transport in the core. However, to compare quantitatively the effects of various mechanisms involved, such as the mentioned role of Te/Ti on ITG turbulence, it is necessary to have primarily simulations of transport codes coupled with first-principle turbulence codes that match both the fluxes and the experimental profiles within experimental uncertainties. This effort is presenly in progress.

3. FILD MEASUREMENTS OF NBI-INDUCED REDUCTION OF FAST-ION LOSSES DURING ECRF AND ICRF HEATING

The primary way to cope with the unfavourable consequences on transport and on PFC integrity due to fast-ion losses induced by shear Alfvén waves [27] excited by fusion alphas in a reactor, is the suppression or, at least, strong mitigation of TAEs and RSAEs with the actuators reviewed in [28]. However, it might be still necessary to envisage methods that reduce fast-ion losses in the presence of "residual" Alfvénic activity, when it is not possible to suppress TAEs and RSAEs completely. With heating systems that can directly modify the fast ion population, such as ICRF and NBI, it is in principle possible to partially tailor the fast-ion distribution function in such a way to reduce the fast-ion losses [28]. This has been recently investigated on ASDEX Upgrade, and figure 4.a shows a few time traces of one of these discharges, 39573, characterized by 2.5 T on-axis magnetic field and 0.7 MA of plasma current. To keep α_c low enough for the existence of TAEs, counter-ECCD at $\rho_{\rm pol} \approx 0.5$ is applied during the whole discharge. About 4 MW of ICRF at 36.5 MHz for core ICRF heating of H minority ($\approx$ 8 %) in deuterium plasmas is applied during the whole discharge flattop. ICRF power is mainly absorbed by H ($\approx$ 80%), and is reduced of about 10% during the NBI-D phases. TAE excitation is clearly caused by ICRF accelerated H, since TAEs appear when ICRF power is ramped-up at the beginning of the phase, and they are present also in phases without NBI heating. At each EC-power

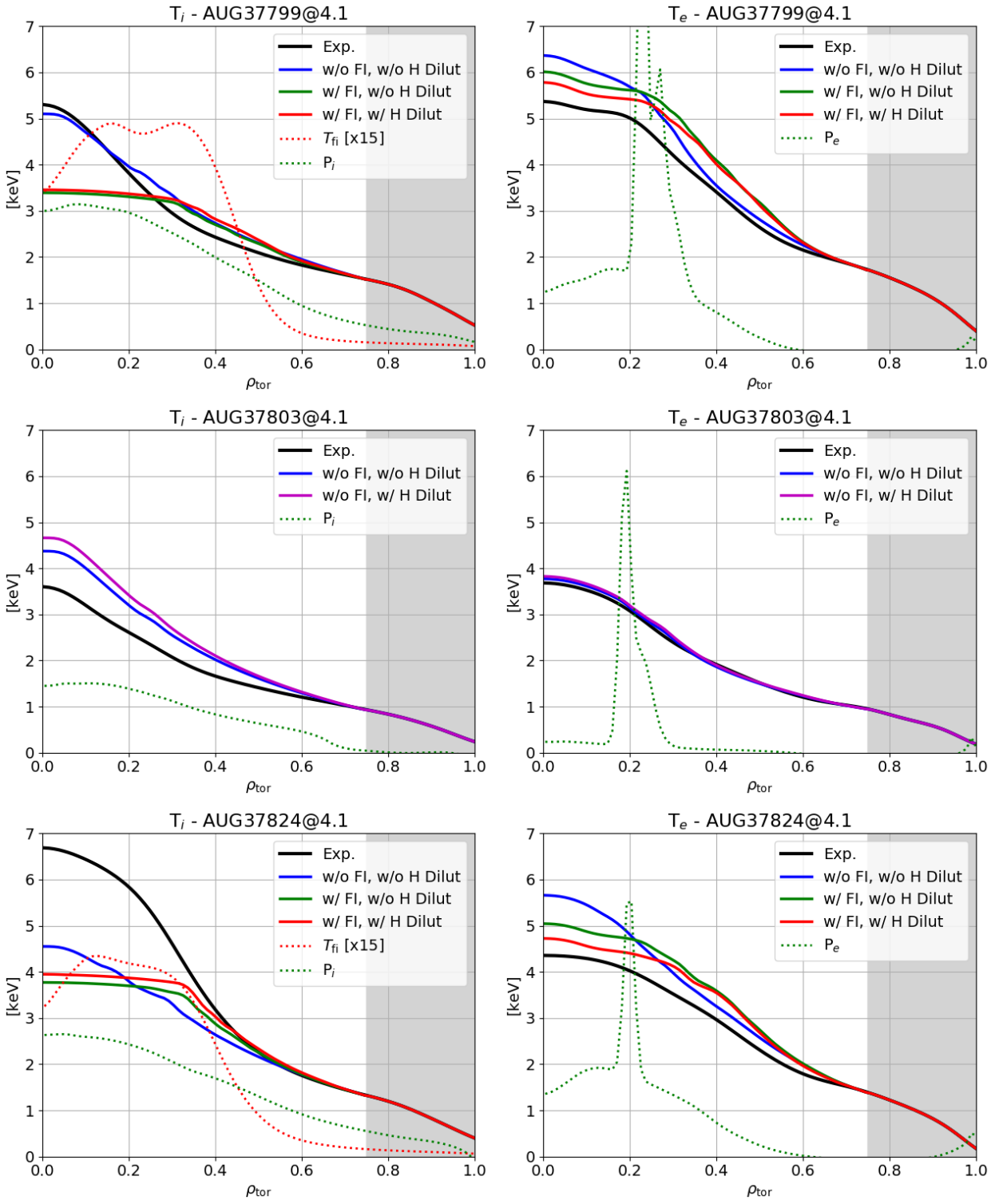

FIGURE 3. Experimental and predicted T_i and T_e profiles for the three discharges 37799, 37803, and 37824.

step there is a 0.9 s phase of NBI heating with source 3 at $\approx$ 59 kV of injection voltage (the same phenomenology has been observed in 38017 during blips of source 8 at $\approx$ 92 kV). During NBI heating the kinetic profiles and plasma

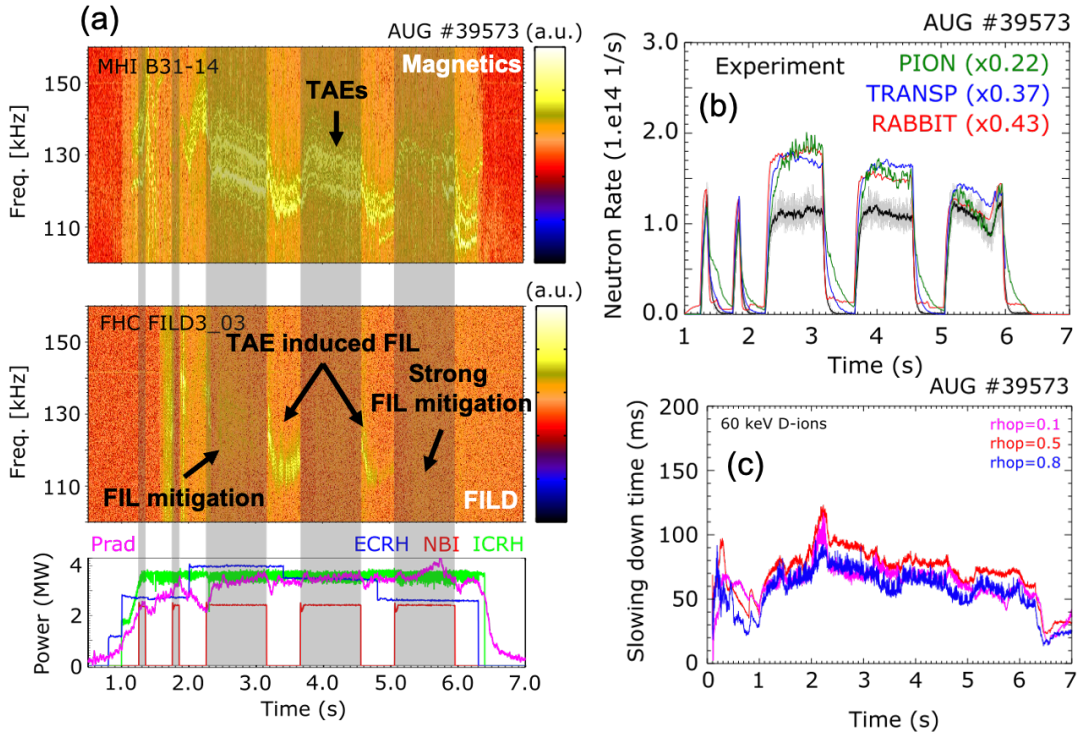

FIGURE 4. (a) Magnetic and FI spectrograms with the heating time traces shown in bottom frame; (b) Experimental neutron-rate measurements with the predictions of three codes, which do not account for TAE fast-ion losses. (c) time traces of the slowing-down time for three radial positions.

toroidal rotation vary with a clear impact on the TAE structure, i.e. on frequency and mode numbers. Despite these changes, TAEs are present during the whole discharge flattop and their amplitude seems to be more sensitive to the EC power step-down than to the NBI heating. Instead, the signal of the fast-ion detector is sensibly reduced during NBI-heating phases. Strictly speaking, this implies only that the portion of the phase space observed by the fast-ion loss detector (FILD) diagnostics is sensibly affected by NBI-heating at the point to have a clear reduction of the losses. The FIDA/BES ratio provides an estimate of the fast-ion density profile. A depletion of this profile at the expected TAE radial location is observed during the first NBI phase, when the TAE amplitude is larger, which seems consistent with the FILD measurements. Additionally, a further hint comes from the comparison between the measured neutron rate in the three NBI-heating phases with what predicted by PION [29], TRANSP [30], and RABBIT [31] codes, which do not take into account collective fast-ion losses due to TAEs, see 4.b During the EC-power step-down, the electron temperature decreases, and this typically decreases the neutron rate from NBI. Mainly for this reason the neutron-rate predicted by the three codes decreases. However, the fact that the experimental measurement stays almost constant in the three NBI phases might be read as a hint of the reduction of NBI-D losses, which counter-balances the effects of T_e reduction, such as the slowing-down time, see 4.c. The hypothesis, which is presently under investigation with different codes, is that NBI-D population enters in competition with H for ICRF direct absorption, and this might be strong enough to have an impact on the distribution function of the ion species (both D and H) at energy far above the thermal bulk [32]. Additionally, changes of the plasma profiles can impact the AE structure in such a way to make fast-ion losses detected by FILD more sensitive to variations of the RF power redistribution with and without NBI. In practice, all this might offer a possible way to externally tailor the distribution function of energetic ions to reduce their losses due to TAE and RSAE and at the same time to let them thermalize.

4. ICE MEASUREMENTS OF GAE

High-frequency Alfvénic activity identified with counter-propagating global Alfvén eigenmodes (GAE) has been observed in NSTX during NBI heating, and it is considered responsible for the electron confinement deterioration with NBI power [5]. These modes belong to the shear branch of the MHD waves with sub-cyclotron frequencies $\omega/\Omega_{ci} \gtrsim 0.5$ (i.e. in the range of a few MHz for typical plasma parameters). Contrary to the low-frequency branches of MHD waves (a few hundreds of kHz), i.e. TAEs and RSAEs, which are destabilized by gradients in space of the fast-ion population, the growth rate of GAE as well as its counter-part, the compressional Alfvén eigenmode (CAE), depends strongly on the gradients in velocity space of the fast-ion distributions [33, 34]. In the limit $k_\perp/k_\parallel \ll 1$ the frequency of the most unstable counter-GAEs is in the range $(1+v_b/v_A)^{-1} < \omega/\omega_{ci} \leq [1+(v_b/v_A)\sqrt{1-\lambda_b}]^{-1}$ with $v_A = B/\sqrt{4\pi m_i n_i}$ the Alfvén speed, v_b the fast-ion velocity, and $\lambda_b = v_{b\perp}^2/v_b^2$ of the fast-ion beam [35]. Analogous high-frequency MHD activity has been observed in DIII-D [36], JT-60U [37], and AUG [38] tokamaks, where these modes have been detected with magnetic B-dot probes, also called ion-cyclotron-emission (ICE) diagnostics. This sensitivity on the λ-gradient of the distribution function predicted by theory [33] is visible in the discharge 38814 of AUG where different NBI sources are singularly active for ≈ 1 s, except for source S4 which is active for almost the whole discharge, since it is the one that excites these modes the most. The ICE spectrogram of this discharge is shown in Figure 5. In this discharge $B_0 \approx 1.6$ T and the core density is about $6 \cdot 10^{19}$ m^{-3}, thus sources S2-S4 and sources S5-S8 have $v_b/v_A \approx 0.75$ and $v_b/v_A \approx 0.95$, respectively. The most tangential (and also with most off-axis

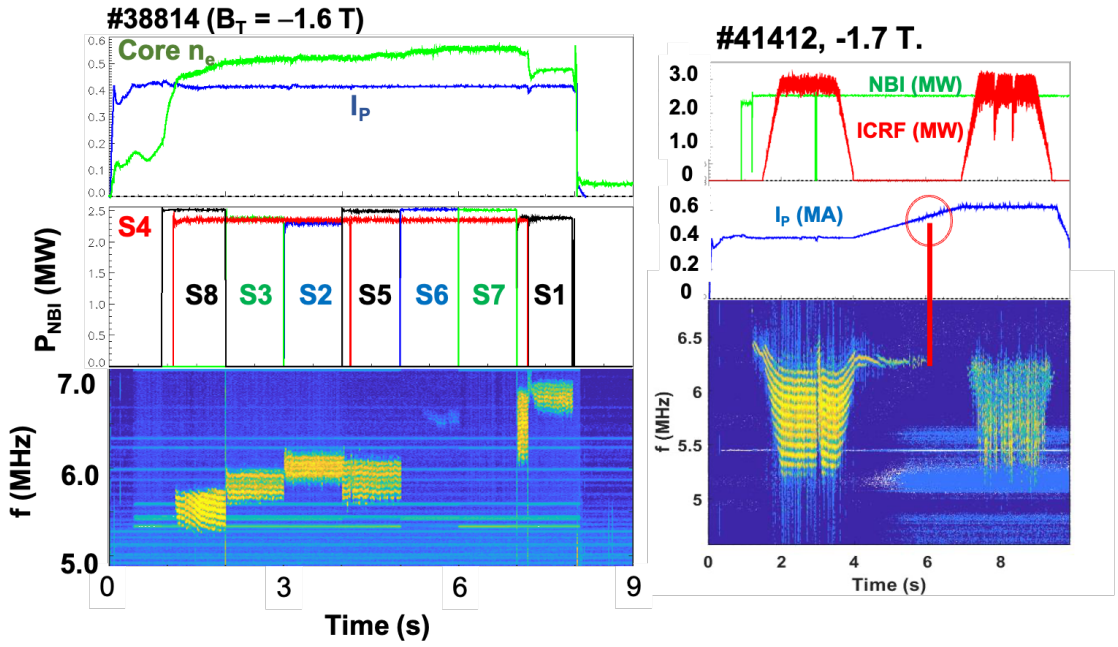

FIGURE 5. ICE spectrogram (a) in the case of scan over the NBI sources on AUG. (b) in the simultaneous presence of ICRF for two values of the plasma current, I_p - in the middle of the discharge there is a ramp-up of I_p and at about 0.55 MA the GAE modes induced by NBI fast ions are stabilized.

deposition) sources, i.e. source 6 and 7, typically do not excite GAEs, and in the case of 38814 they even stabilized GAEs due to S4. This behaviour agrees with the nonlinear modeling which highlights the different roles that resonant fast ions can have on stabilizing or destabilising these modes depending on their pitch angle, $v_{b\parallel}/v$ [33]. It is also interesting to observe that at the end of the discharge there are two phases, one with S4 plus S1 and the last with S1 only. The spectra are substantially different and cannot be interpreted as a simple superimposition of individual spectra. This confirms the numerical analysis that GAE growth rates depend on the net contribution of the fast-ion distribution function in a rather involved way as a result of the competition between resonant stabilizing and resonant destabilizing fast ions [33]. The peculiarity of AUG with respect to the other tokamaks where these modes have been studied so far is the possibility of studying the effects of high-harmonic (i.e. 2nd, 3rd, 2nd+3rd) ICRF heating on

GAEs. Heating at IC resonances above the fundamental is a finite-Larmor effect and thus it preferentially accelerates energetic ions with large $k_\perp \rho$, with $\rho = v/\Omega_{ci}$ the Larmor radius. Therefore, ICRF can modify the NBI-D distribution function by increasing the fast ion energy, preferentially in the direction perpendicular to the confining magnetic field (i.e. increasing λ_b, roughly speaking). The consequence is that more modes are expected to be excited, as it is indeed the case according to ICE measurements [39]. Figure 5 shows the ICE spectrogram together with time traces of ICRF and NBI heating for 41412 (1.6T/0.6MA). ICRF frequency is 36.5 MHz with the 3rd harmonic of D in the plasma core. At the 3rd harmonic of D there is no competition with a parasitic absorption by H, whose concentration in these discharges is anyway rather low, $\lesssim 1\%$. In the first ICRF phase, ICE spectrum follows closely the waveform of ICRF power, P_{ic}, and during the ramp-up and ramp-down of P_{ic} the number of modes that are de-stabilized increases and decreases, respectively. This is mainly due to the fact that the distortion of the fast-ion distribution function depends on P_{ic}, and by increasing the anisotropy in λ more modes can resonate with the fast ions. This feature with P_{ic} is robust and reproducible on AUG. An other important aim of this discharge was to assess the effect of I_p in stabilizing GAEs. By increasing I_p, the safety factor decreases, and it enters explicitly in the wave-particle resonance condition. With this aim, in the middle of the discharge I_p is increased from ≈ 0.4 MA to ≈ 0.6 MA. At about 0.55MA the GAEs modes disappear completely in the ICE spectrogram, and they reappear only later during the last ICRF heating phase, similar to the first ICRF phase. Detailed analysis with numerical codes is in progress and will be reported in a future work.

5. CONCLUSIONS

The physics of fast ions is crucial in burning plasmas, and consequently it is fundamental to address their effects in present devices. ICRF heating, in combination also with NBI, offers a unique tool to generate/control fast ions. Although there are key differences with respect to fusion alphas, e.g. the anisotropy in velocity space, ICRF accelerated ions are a valuable proxy of fusion alphas in present devices, especially in view of improving and verifying models and validating codes. Additionally, ICRF and NBI are essential heating systems in ITER to enter H mode and to reach burning plasma conditions. Therefore, an integrated use of the positive effects of ICRF/NBI fast ions on reduction/control of core turbulence might help to improve the path to burning-plasma phase. We have shown on AUG shots that reduced models, such as TGLF, are capable to describe some of the FI effects on transport. However, TGFL in ASTRA seems not to be able to reproduce the differences between 37799 and 37824 which look rather similar except for the ECRF power. This might be due to the fact that only global gyrokinetic simulations properly describe the FI effects on transport, and this might naturally limit the capability of present reduced models (typically local) in accounting for FI effects.

From the specific comparison between these two shots (and from other not reported here), we have observed that when $T_i \approx T_e$ a further increase of ECRF power deteriorates the ion confinement, precisely reduces T_i. This requires further investigation, and also might imply that an optimized path to high-performance plasmas in ITER will require a controlled mixture of the three auxiliary heating systems, i.e. ECRF, NBI and ICRF.

AUG discharges show that NBI can reduce ICRF fast-ion losses due to TAEs, which in turn are excited by the same ICRF fast ions. In this specific case, ICRF fast ions mimic the fusion alphas, and NBI is the actuator to modify the "fusion-alpha" distribution function in order to reduce their losses. In the future it is important to understand how far it is possible to envisage a suitable use of NBI in combination with ICRF to mitigate these fast ion losses in view of ITER and future fusion devices. Finally, ICRF and NBI fast ions are crucial to study in tokamaks the effects on electron confinement of high-frequency MHD modes, such as GAEs. We have discussed AUG shots where ICRF acceleration of NBI-D was used to extend the spectrum of GAE modes, detected with an array of B-dot probes, and to excite them when they were stable (when plasma current was above the threshold).

ACKNOWLEDGMENTS

We wish to acknowledge M. Bergmann, M. Brambilla, P. David, R. Mc Dermott, Ph. Lauber, U. Plank, M. Reisner, S. Sharapov, G. Staebler, G. Tardini, E. Viezzer, B. Zimmermann, and to thank A. Kappatou, E. Tsitrone and A. Hakola for their kind support. J. Galdon-Quiroga acknowledges funding from the Spanish Ministry of Science and Innovation under grant no. FJC2019-041092-I.

See the author list of U. Stroth et al. 2022 Nucl. Fusion **62** 042006 for the ASDEX Upgrade Team; see the author list of B. Labit et al. 2019 Nucl. Fusion **59** 086020 for the EUROfusion MST1 team.

This work has been carried out within the framework of the EUROfusion Consortium, funded by the European Union via the Euratom Research and Training Programme (Grant Agreement No 101052200 — EUROfusion). Views and opinions expressed are however those of the author(s) only and do not necessarily reflect those of the European Union or the European Commission. Neither the European Union nor the European Commission can be held responsible for them.

REFERENCES

1. M. Schneider, A. Polevoi, S. Kim, A. Loarte, S. Pinches, J.-F. Artaud, E. Militello-ASP, B. Beaumont, R. Bilato, D. Boilson, et al., Nuclear Fusion **59**, 126014 (2019).
2. J. Garcia, Plasma Physics and Controlled Fusion **64**, 104002 (2022).
3. J. Citrin and P. Mantica, Submitted to Plasma Physics Controlled Fusion (2022).
4. A. D. Siena, T. Görler, H. Doerk, E. Poli, and R. Bilato, Nuclear Fusion **58**, 054002 (2018).
5. D. Stutman, L. Delgado-Aparicio, N. Gorelenkov, M. Finkenthal, E. Fredrickson, S. Kaye, E. Mazzucato, and K. Tritz, Phys. Rev. Lett. **102**, 115002 (2009).
6. M. Usoltseva, R. Bilato, V. Bobkov, M. Weiland, H. Faugel, H. Fünfgelder, R. Ochoukov, O. Samoylov, and the ASDEX Upgrade team, in *This conference* (2022).
7. L. Chen and F. Zonca, Phys. Rev. Lett. **109**, 145002 (2012).
8. B. N. Rogers, W. Dorland, and M. Kotschenreuther, Phys. Rev. Lett. **85**, 5336 (2000).
9. G. G. Whelan, M. J. Pueschel, and P. W. Terry, Phys. Rev. Lett. **120**, 175002 (2018).
10. A. Di Siena, T. Görler, E. Poli, A. Bañón Navarro, A. Biancalani, R. Bilato, N. Bonanomi, I. Novikau, F. Vannini, F. Jenko, et al., Journal of Plasma Physics **87**, 555870201 (2021).
11. G. Y. Fu, Physics of Plasmas **2**, 1029 (1995).
12. S. Mazzi, J. Garcia, D. Zarzoso, Y. O. Kazakov, J. Ongena, M. Dreval, M. Nocente, Z. Stancar, G. Szepesi, J. Eriksson, et al., Nat. Phys. **18**, 776–782 (2022).
13. S. Günter, A. Gude, J. Hobirk, M. Maraschek, S. Saarelma, S. Schade, R. Wolf, and A. U. Team, Nuclear Fusion **41**, 1283 (2001).
14. S. D. Pinches, S. Günter, and A. G. Peeters, in *28th EPS conference* (2001), vol. 25A.
15. A. Di Siena, T. Görler, E. Poli, R. Bilato, H. Doerk, and A. Zocco, Physics of Plasmas **26**, 052504 (2019).
16. G. M. Staebler, J. Candy, N. T. Howard, and C. Holland, Physics of Plasmas **23**, 062518 (2016).
17. T. Stix, Nuclear Fusion **15**, 737 (1975).
18. P. Mantica, C. Angioni, C. Challis, G. Colyer, L. Frassinetti, N. Hawkes, T. Johnson, M. Tsalas, P. C. deVries, J. Weiland, et al., Phys. Rev. Lett. **107**, 135004 (2011).
19. M. J. Mantsinen, R. Bilato, V. V. Bobkov, A. Kappatou, M. R. M., M. Nocente, T. Odstrčil, G. Tardini, M. Bernert, R. Dux, et al., AIP Conference Proceedings **1689**, 030005 (2015).
20. P. David, M. Bernert, T. Pütterich, C. Fuchs, S. Glöggler, T. Eich, and the ASDEX Upgrade Team, Nuclear Fusion **61**, 066025 (2021).
21. A. Di Siena, R. Bilato, T. Görler, A. B. n. Navarro, E. Poli, V. Bobkov, D. Jarema, E. Fable, C. Angioni, Y. O. Kazakov, et al., Phys. Rev. Lett. **127**, 025002 (2021).
22. O. Kudlacek, T. Bosman, F. Felici, L. Giannone, S. van Mulders, O. Sauter, B. Sieglin, W. Treutterer, N. Vu, M. Weiland, et al., Fusion Engineering and Design **171**, 112563 (2021), ISSN 0920-3796.
23. E. Joffrin, G. Gorini, C. D. Challis, N. C. Hawkes, T. C. Hender, D. F. Howell, P. Maget, P. Mantica, D. Mazon, S. E. Sharapov, et al., Plasma Physics and Controlled Fusion **44**, 1739 (2002).
24. E. Poli, A. Bock, M. Lochbrunner, O. Maj, M. Reich, A. Snicker, A. Stegmeir, F. Volpe, N. Bertelli, R. Bilato, et al., Computer Physics Communications **225**, 36 (2018).
25. R. Bilato, M. Brambilla, O. Maj, L. Horton, C. Maggi, and J. Stober, Nuclear Fusion **51**, 103034 (2011).
26. P. N. Y. G. Pereverzev, Tech. Rep. IPP 5/42, Mak-Planck-Institut für Plasmaphysik (1991).
27. H. Duong, W. Heidbrink, E. Strait, T. Petrie, R. Lee, R. Moyer, and J. Watkins, Nuclear Fusion **33**, 749 (1993).
28. M. Garcia-Munoz, S. E. Sharapov, M. A. V. Zeeland, E. Ascasibar, A. Cappa, L. Chen, J. Ferreira, J. Galdon-Quiroga, B. Geiger, J. Gonzalez-Martin, et al., Plasma Physics and Controlled Fusion **61**, 054007 (2019).
29. L.-G. Eriksson, T. Hellsten, and U. Willen, Nuclear Fusion **33**, 1037 (1993).
30. `TRANSP`, https://doi.org/10.11578/dc.20180627.4.
31. M. Weiland, R. Bilato, R. Dux, B. Geiger, A. Lebschy, F. Felici, R. Fischer, D. Rittich, M. van Zeeland, and and, Nuclear Fusion **58**, 082032 (2018).
32. J.-Q. et al, in preparation (2022).
33. E. V. Belova, E. D. Fredrickson, J. B. Lestz, and N. A. Crocker, Physics of Plasmas **26**, 092507 (2019).
34. J. B. Lestz, N. N. Gorelenkov, E. V. Belova, S. X. Tang, and N. A. Crocker, Physics of Plasmas **27**, 022513 (2020).
35. E. Belova, N. A. Crocker, J. Lestz, and E. Fredrickson, Nuclear Fusion (2022).
36. W. Heidbrink, E. Fredrickson, N. Gorelenkov, T. Rhodes, and M. V. Zeeland, Nuclear Fusion **46**, 324 (2006).
37. S. Sumida, K. Shinohara, M. Ichimura, T. Bando, A. Bierwage, and S. Ide, Nuclear Fusion **61**, 116036 (2021).
38. R. Ochoukov, R. Bilato, V. Bobkov, S. Chapman, R. Dendy, M. Dreval, H. Faugel, A. Kappatou, Y. Kazakov, M. Mantsinen, et al., Nuclear Fusion **60**, 126043 (2020).
39. R. Ochoukov, S. Sipilä, R. Bilato, V. Bobkov, M. Dreval, M. Weiland, R. Dendy, H. Faugel, T. Johnson, A. Kappatou, et al., accepted in Nuclear Fusion (2023).